Model-Based Predictive Impedance Variation for Obstacle Avoidance in Safe Human–Robot Collaboration

Salt Ducaju, Julian; Olofsson, Björn; Johansson, Rolf

Published in:
IEEE Transactions on Automation Science and Engineering

DOI:
10.1109/TASE.2024.3508718

2025

Document Version:
Peer reviewed version (aka post-print)

Model-Based Predictive Impedance Variation for Obstacle Avoidance in Safe Human–Robot Collaboration

Julian M. Salt Ducaju, Björn Olofsson, Rolf Johansson

***Abstract*—Human–robot collaboration (HRC) in manufacturing environments requires that physical safety can be guaranteed. Control methods that implicitly regulate the interaction forces between a controlled robot and its environment, such as impedance control, are often used for safety in HRC. However, these methods could be complemented by restricting the robot operational space for additional safety guarantees. In this context, obstacle avoidance might benefit from considering a prediction of the controlled-robot motion and/or the behavior of the human collaborator. To this end, we proposed to include linearized Safety Control Barrier Functions (SCBFs) in a linear Model Predictive Control (MPC) strategy for robot impedance variation online. The convex optimization problem that was obtained from our proposal presented two advantages compared to nonlinear MPC alternatives. First, optimality was ensured in our method under linearity assumptions on human guidance and linearized robot dynamics, whereas a controller synthesized by nonlinear MPC strategies would depend on the fundamental characteristics of the problem. Second, our method enabled implementation at a faster control frequency, thus allowing a rapid adaptation to changes occurring in the robot environment. Finally, experimental validation was performed using a Franka Emika Panda robot in a human–robot collaborative scenario, and the stability of the method was shown using Lyapunov theory.**

***Note to Practitioners*—Modern-day industrial manufacturing environments are characterized by collaboration between human operators and robot manipulators. In this scenario, where humans and robots share workspace, physical safety is required. This research aims to improve safety in human–robot collaboration by proposing a novel robot control strategy. In our approach, the interaction forces between the controlled robot and its environment were regulated implicitly using impedance control, to allow, among other interactions, that an operator could manually guide the robot. Then, obstacle avoidance was included to modify the robot impedance behavior for restricting undesired collisions with, for example, the operator head, while ensuring stability of the method. Our main contribution is that the proposed formulation allows to consider a prediction of the robot motion and/or the operator behavior for robot obstacle avoidance. It was shown in experiments with a real robot that adding prediction capabilities reduced the risk of undesired collisions, while also decreasing the robot trajectory error. Moreover, the method could be implemented at a fast rate so that the robot could react rapidly to changes in its environment. Also, this implementation allowed to achieve a minimal variation with respect to the nominal impedance behavior of the robot. To conclude, this method is intended for scenarios where a robot is required to interact with its, possible restricted, environment: for example, a robot with a drill attached to its end-effector that is being guided to modify its trajectory, but where the operator should not be allowed to accidentally be harmed; or a robot performing a polishing task where a section of the polished object should remain unpolished. Therefore, using the proposed robot control strategy, a possible extension of this research would be to provide an improved prediction of the human operator intention depending on the desired robotic task and the role of the operator.**

***Index Terms*—Physical human–robot interaction (pHRI), robot safety, Model Predictive Control (MPC), impedance control, Safety Control Barrier Functions (SCBFs).**

The authors are members of the ELLIIT Strategic Research Area at Lund University. This work was partially supported by the Wallenberg AI, Autonomous Systems and Software Program (WASP).

J. M. Salt Ducaju, julian.salt_ducaju@control.lth.se, B. Olofsson, and R. Johansson are with the Department of Automatic Control, LTH, Lund University, Lund, Sweden. B. Olofsson is also affiliated with the Division of Vehicular Systems, Department of Electrical Engineering, Linköping University, Linköping, Sweden.

Fig. 1. A human–robot collaborative scenario where an operator was guiding a Franka Emika Panda robot mounted on a table.

I. Introduction

Former industrial settings, characterized by a fixed-structure workspace, present limitations when addressing current manufacturing trends, in which mass production has been replaced for mass customization, *i.e.*, smaller volumes of products are manufactured during shorter time frames [1]. As an attempt to improve human contribution, in terms of intelligence, dexterity, and responsiveness, in this rapidly changing industrial

environment, human–robot collaboration (HRC) has increased its relevance in recent years [2]. Several methods for HRC involve a physical interaction between humans and robots (pHRI), such as kinesthetic teaching, where human guidance is used to modify a robot trajectory [3]; or human–robot cooperation, where a robot provides proactive assistance to a human operator [4].

The most important requirement of any collaborative manufacturing scenario is that physical safety can be guaranteed for all humans, robots, and any other actor present in the shared workspace. To achieve this, indirect force control methods, such as impedance control [5], [6], are often used. Impedance control improves physical safety in HRC by implicitly regulating the interaction forces between the controlled robot and its environment, which also allows physical guidance of the robot. However, the interaction-force regulation achieved by an impedance-control strategy might not be sufficient to ensure safety in HRC applications, *e.g.*, if fragile equipment was located in the shared workspace, or if further protection was desired for the most sensitive body parts of human operators, such as their heads. In these scenarios, it is necessary to constrain the available operational space of the robot by creating restricted zones that the robot should avoid.

Safety Control Barrier Functions (SCBFs) [7] have been extensively used in recent years to bound the operational space of robot manipulators [8]–[12] since they provide formal forward-invariance conditions to ensure that a robot does not leave a safe set of states, *i.e.*, a robot that started its motion in its allowed operational space would not invade a restricted zone. To achieve a minimally-invasive modification of the nominal behavior of the robot, SCBFs have been included as inequality constraints in a quadratic optimization problem whose goal was to minimize the difference between a nominal control signal and a control signal that would satisfy the safety requirements imposed by the SCBFs [7]. Convexity guarantees in this formulation ensured optimality, and allowed a fast execution of this safety strategy at the sampling frequency of the controlled robot, which can be as fast as 1 kHz. Moreover, in the context of HRC, SCBFs have been considered to adapt the acceleration of a robot depending on a human–robot separation distance [10], resulting in a safety improvement for human–robot contacts. Then, regarding safety in pHRI, SCBFs have been considered to modify an impedance control structure for robot obstacle avoidance [11], [12].

Furthermore, so far, SCBF-based proposals to constrain the operational space of robot manipulators [8]–[12] have been formulated as 1-step quadratic optimization problem, thus not containing prediction capabilities regarding robot motion and/or the behavior of the operator. The advantages of prediction for collision avoidance have been studied for other types of robotic systems, such as legged robots [13] and mobile robots [14], where SCBFs were combined with Model Predictive Control (MPC) strategies to include longer temporal-horizon predictions for safety improvement. However, nonlinear MPC strategies were proposed in [13], [14], which caused their optimization problem to depend on the fundamental characteristics of the problem, thus no guarantees for global optimality could be provided from the obtained solution. Additionally, the longer computational times of the nonlinear MPC strategies prevented their implementation executing at a fast rate, hence reducing the robot capacity to react to changes in their environment, which is especially relevant in safety-related robotic scenarios.

In this paper, we address the problem of improving safety in HRC by considering a longer temporal-horizon prediction of the behavior of both the controlled robot and the human operator involved. To this end, we propose to vary the impedance behavior of a robot manipulator using a linear MPC strategy that includes the forward-invariance condition of a SCBF that is linearized at each time-step. This MPC formulation presented results in a convex quadratic optimization problem that could be solved at the control rate of a real robot (1 kHz), while ensuring optimality in the proposed method under linearity assumptions on human guidance and linearized robot dynamics. Additionally, a Lyapunov function is used to provide global asymptotic stability guarantees and real experiments were performed to evaluate the method on a robot.

The paper is organized as follows: Sec. II introduces the dynamics model used for impedance control of the robot manipulator. Then, Sec. III presents a linearized barrier function for robot obstacle avoidance, which is used as a linear inequality constraint in the optimization problem developed in Sec. IV for safe human–robot collaboration. The method proposed in Sec. IV was evaluated in simulations, included in Section V, and experiments with a real robot, presented in Section VI. Finally, a discussion is included in Sec. VII and conclusions are drawn in Sec. VIII.

II. Modeling

First, we show how a Cartesian impedance controller acting on the rigid-body dynamics of a robot can be written as a Linear Parameter-Varying (LPV) model.

A. Robot Rigid-Body Dynamics

The rigid-body dynamics of the robot can be written in the joint space of the robot, $q \in \mathbb{R}^n$, as [15]

$$M(q)\ddot{q} + C(q,\dot{q})\dot{q} + G(q) = \tau + \tau^{\text{ext}} \tag{1}$$

where $M(q) \in \mathbb{R}^{n\times n}$ is the generalized inertia matrix, $C(q,\dot{q}) \in \mathbb{R}^{n\times n}$ describes the Coriolis and centripetal forces effects, $G(q) \in \mathbb{R}^n$ captures the gravity-induced torques, and $\tau \in \mathbb{R}^n$ represents the input torques, n being the number of joints of the robot. Finally, $\tau^{\text{ext}} \in \mathbb{R}^n$ represents the external torques.

Moreover, the rigid-body equation of the robot can be rewritten in terms of its end-effector pose $\xi \in \mathbb{R}^m$ which is composed by the end-effector's position and orientation:

$$M_\xi(q)\ddot{\xi} + C_\xi(q,\dot{q})\dot{\xi} + G_\xi(q) = F + F^{\text{ext}} \tag{2}$$

where $F \in \mathbb{R}^m$ is the input force, and, for a fully-actuated nonredundant robot ($n = m$), $M_\xi \in \mathbb{R}^{m\times m}$, $C_\xi \in \mathbb{R}^{m\times m}$, and $G_\xi \in \mathbb{R}^m$ are equal to

$$M_\xi = J^{-\text{T}}(q)M(q)J^{-1}(q) \tag{3}$$

$$C_\xi = J^{-\text{T}}(q)(C(q,\dot{q}) - M(q)J^{-1}(q)\dot{J}(q,\dot{q}))J^{-1}(q) \tag{4}$$

$$G_\xi = J^{-\text{T}}(q)G(q) \tag{5}$$

assuming that the Jacobian relative to the base frame of the robot, $J(q) \in \mathbb{R}^{m\times m}$, has full rank [16]; see [17] for a review of Jacobian inversion techniques in the neighborhood of singular joint configurations.

B. Robot Impedance Control

To achieve a Cartesian impedance control of the robot end-effector [5], [6], *i.e.*, a mass-spring-damper relationship between the Cartesian pose variation from its reference, $\Delta\xi = \xi_d - \xi$ (ξ_d being the Cartesian pose reference) and the external Cartesian force F^{ext},

$$F^{\text{ext}} = M_\xi(q)\ddot{\xi} + (C_\xi(q,\dot{q}) + D)\dot{\xi} - K\Delta\xi \tag{6}$$

the input force F in Eq. (2) should be equal to

$$F = K\Delta\xi - D\dot{\xi} + G_\xi(q) \tag{7}$$

where $K \in S^m_{++}$ and $D \in S^m_{++}$ (S_{++} denoting symmetric positive-definiteness) are diagonal matrices that represent the control-induced stiffness and damping, respectively.

Remark. *The control-induced inertia was chosen equal to the robot inertia $M_\xi(q)$ to avoid inertia shaping [18, Ch. 3.2], so that the input force F would not require feedback from the external forces.*

Moreover, by choosing the state vector as $x = [\Delta\xi^{\mathrm{T}}, \Delta\dot{\xi}^{\mathrm{T}}]^{\mathrm{T}} \in \mathbb{R}^{2m}$, the linearized system is

$$\dot{x} = A(q,\dot{q})x + B(q)u \tag{8}$$

where the input $u \in \mathbb{R}^m$ is equal to

$$u = F^{\text{ext}} \tag{9}$$

and the matrices that define the system are equal to

$$A = \begin{bmatrix} 0_m & I_m \\ -M_\xi^{-1}(q)K & -M_\xi^{-1}(q)(C_\xi(q,\dot{q}) + D) \end{bmatrix} \tag{10}$$

$$B = \begin{bmatrix} 0_m \\ -M_\xi^{-1}(q) \end{bmatrix} \tag{11}$$

where $I_m \in \mathbb{R}^{m\times m}$ represents an identity matrix, and $M_\xi(q)$ is invertible since $J(q)$ is also invertible [12, Lemma III.1].

Furthermore, the impedance control resulting in Eq. (8) has shown to be globally asymptotically stable [12]. For completeness, a short version of the proof is provided here, see [12, Lemma III.2] for an extended version of this proof.

Proposition 1. *The time-varying Lyapunov function*

$$V(x,t) = \frac{1}{2}\Delta\dot{\xi}^{\mathrm{T}}M_\xi(q)\Delta\dot{\xi} + \frac{1}{2}\Delta\xi^{\mathrm{T}}K\Delta\xi + \alpha\Delta\xi^{\mathrm{T}}M_\xi(q)\Delta\dot{\xi} \tag{12}$$

where $x = \left[\Delta\xi^{\mathrm{T}}, \Delta\dot{\xi}^{\mathrm{T}}\right]^{\mathrm{T}}$ shows the global asymptotic stability of the impedance robot behavior in Eq. (6) for $\alpha > 0$ satisfying

$$\min\Big(\sqrt{\frac{\lambda_{m,K}}{\lambda_{M,M_\xi}}},\ \frac{2\lambda_{m,K}}{\lambda_{M,D}},\ \frac{\lambda_{m,D}}{2(\lambda_{M,M_\xi} + k_C||\Delta\xi||)}\Big) > \alpha \tag{13}$$

where $\lambda_{m,\Pi}$ and $\lambda_{M,\Pi}$ are the smallest and largest eigenvalues of a matrix Π, respectively, and k_C is a positive constant such that for all $x, y, z \in \mathbb{R}^n$ [19]

$$||C_\xi(x,y)z|| \le k_C||y||||z|| \tag{14}$$

Proof. The Lyapunov candidate (12) is strictly positive for

$$\alpha < \sqrt{\frac{\lambda_{m,K}}{\lambda_{M,M_\xi}}} \tag{15}$$

Moreover, considering that the matrix $\dot{M}_\xi(q) - 2C_\xi(q,\dot{q})$ is skew symmetric [18, Ch. 2], the time-derivative of the Lyapunov candidate (12) is equal to

$$\begin{aligned}\dot{V}(x) = &-\alpha\Delta\xi^{\mathrm{T}}C_\xi(q,\dot{q})\Delta\dot{\xi} + \alpha\Delta\dot{\xi}^{\mathrm{T}}M_\xi(q)\Delta\dot{\xi} \\ &-\Delta\dot{\xi}^{\mathrm{T}}D\Delta\dot{\xi} - \alpha\Delta\xi^{\mathrm{T}}K\Delta\xi + \alpha\Delta\xi^{\mathrm{T}}D\Delta\dot{\xi}\end{aligned} \tag{16}$$

Then, defining the upper bound on certain terms:

$$-\Delta\dot{\xi}^{\mathrm{T}}D\Delta\dot{\xi} \le -\frac{1}{2}\Delta\dot{\xi}^{\mathrm{T}}D\Delta\dot{\xi} - \frac{1}{2}\lambda_{m,D}\big||\Delta\dot{\xi}\big||^2 \tag{17}$$

$$\alpha\Delta\dot{\xi}^{\mathrm{T}}M_\xi(q)\Delta\dot{\xi} \le \alpha\lambda_{M,M_\xi}\big||\Delta\dot{\xi}\big||^2 \tag{18}$$

$$-\alpha\Delta\xi^{\mathrm{T}}C_\xi(q,\dot{q})\Delta\dot{\xi} \le \alpha k_C\big||\Delta\xi\big||\big||\Delta\dot{\xi}\big||^2 \tag{19}$$

it follows that

$$\begin{aligned}\dot{V}(x) \le &-\frac{1}{2}\left[\Delta\dot{\xi} - \alpha\Delta\xi\right]^{\mathrm{T}} D\left[\Delta\dot{\xi} - \alpha\Delta\xi\right] \\ &+\alpha\Delta\xi^{\mathrm{T}}\left[\tfrac{\alpha}{2}D - K\right]\Delta\xi - \frac{1}{2}\lambda_{m,D}\big||\Delta\dot{\xi}\big||^2 \\ &+\alpha k_C\big||\Delta\xi\big||\big||\Delta\dot{\xi}\big||^2 + \alpha\lambda_{M,M_\xi}\big||\Delta\dot{\xi}\big||^2\end{aligned} \tag{20}$$

which is equivalent to

$$\dot{V}(x) \le -\frac{1}{2}\left[\Delta\dot{\xi} - \alpha\Delta\xi\right]^{\mathrm{T}} D\left[\Delta\dot{\xi} - \alpha\Delta\xi\right] \tag{21}$$

for

$$\min\Big(\frac{2\lambda_{m,K}}{\lambda_{M,D}},\ \frac{\lambda_{m,D}}{2(\lambda_{M,M_\xi} + k_C||\Delta\xi||)}\Big) > \alpha \tag{22}$$

Therefore, if $\alpha > 0$ satisfies (13), the Lyapunov candidate function $V(x)$ is strictly positive and its time-derivative $\dot{V}(x)$ is strictly negative. □

Additionally, since $M_\xi(q)$, K, $D \in S^m_{++}$, a passive map from the external force F^{ext} to $\Delta\dot{\xi}$ is guaranteed,

$$\begin{aligned}\dot{V} &< \Delta\dot{\xi}^{\mathrm{T}}F^{\text{ext}} - \frac{1}{2}\left[\Delta\dot{\xi} - \alpha\Delta\xi\right]^{\mathrm{T}} D\left[\Delta\dot{\xi} - \alpha\Delta\xi\right] \\ &< \Delta\dot{\xi}^{\mathrm{T}}F^{\text{ext}}\end{aligned} \tag{23}$$

where the passivity condition valid for passive environments is defined analogously

$$V(x,t) - V(x,0) < \int_0^t \Delta\dot{\xi}^{\mathrm{T}}(\tau)F^{\text{ext}}(\tau)\mathrm{d}\tau \tag{24}$$

III. Robot Obstacle Avoidance

Robot obstacle avoidance can be achieved by defining a safe set of robot states and ensuring that the robot would stay inside this set. For this, a barrier function $h : \mathcal{D} \to \mathbb{R}$ was defined for all $x \in \mathcal{D} \subset \mathbb{R}^{2m}$ based on the condition that the distance from the robot position, $\rho(x) \in \mathbb{R}^3$, to an obstacle located at position $\rho_{\text{obs}} \in \mathbb{R}^3$ would always be greater than or equal to a safety distance $D_s \in \mathbb{R}$ as

$$h(x) = ||\rho(x) - \rho_{\text{obs}}|| - D_s \geq 0 \tag{25}$$

which is equivalent to

$$h(x) = (\rho(x) - \rho_{\text{obs}})^2 - D_s^2 \geq 0 \tag{26}$$

The forward-invariance of the safe set $\mathcal{C} \subseteq \mathcal{D}$ defined by the barrier function in (26),

$$\mathcal{C} = \{x \in \mathbb{R}^{2m} \mid h(x) \geq 0\} \tag{27}$$

can be ensured if the following inequality constraint is satisfied [7]

$$\dot{h}(x) + \gamma h(x) \geq 0 \tag{28}$$

where $\gamma > 0$.

Moreover, the forward-invariance condition (28) of the safe set $\mathcal{C}$ can be rewritten for a variable $z = [\rho^{\text{T}}, \dot{\rho}^{\text{T}}]^{\text{T}}$ as a quadratic constraint

$$z^{\text{T}} A_z z + B_z z + C_z \geq 0 \tag{29}$$

where

$$A_z = \begin{bmatrix} \gamma I_3 & I_3 \\ I_3 & 0_3 \end{bmatrix} \tag{30}$$

$$B_z = -2\rho_{\text{obs}}^{\text{T}} \begin{bmatrix} \gamma I_3, & I_3 \end{bmatrix} \tag{31}$$

$$C_z = \gamma(\rho_{\text{obs}}^{\text{T}} \rho_{\text{obs}} - D_s^2) \tag{32}$$

which is equivalent to a quadratic inequality constraint in x

$$x^{\text{T}} A_x x + B_x x + C_x \geq 0 \tag{33}$$

since

$$z = \begin{bmatrix} \rho_d \\ 0_{3\times 1} \end{bmatrix} - T_x x \tag{34}$$

with A_x, B_x, and C_x defined analogous to A_z, B_z, and C_z, and where

$$T_x = \begin{bmatrix} I_3 & 0_3 & 0_3 & 0_3 \\ 0_3 & 0_3 & I_3 & 0_3 \end{bmatrix} \tag{35}$$

and ρ_d is the Cartesian position reference. Also, $0_m \in \mathbb{R}^{m\times m}$ represents a zero matrix, and a zero-velocity reference was assumed.

Furthermore, since including a quadratic constraint would cause an optimization problem to be a Quadratically Constrained Quadratic Program (QCQP), which is NP-hard in its general case, the quadratic inequality constraint (29) was linearized around $z_{\text{int}} = [\rho_{\text{int}}^{\text{T}}, 0]^{\text{T}}$, ρ_{int} being the intersection between the vector $\overrightarrow{\rho_{\text{obs}}\rho}$ and a sphere with center at ρ_{obs} and radius equal to the safety distance D_s. Since this sphere-vector pair would intersect at two points, ρ_{int} would be chosen as the closest of these two points to the position of the robot, ρ. The linearized inequality constraint is equal to

$$(\rho_{\text{int}} - \rho_{\text{obs}})^{\text{T}} \left(\begin{bmatrix} I_3, & \frac{1}{\gamma} I_3 \end{bmatrix} z - \rho_{\text{int}} \right) \geq 0 \tag{36}$$

which is equivalent to a linear inequality constraint in x (34)

$$A_{\text{BF}} x \leq b_{\text{BF}} \tag{37}$$

with

$$A_{\text{BF}} = (\rho_{\text{int}} - \rho_{\text{obs}})^{\text{T}} \begin{bmatrix} I_3, & \frac{1}{\gamma} I_3 \end{bmatrix} T_x \tag{38}$$

$$b_{\text{BF}} = (\rho_{\text{int}} - \rho_{\text{obs}})^{\text{T}} (\rho_d - \rho_{\text{int}}) \tag{39}$$

Remark. *The linear inequality constraint (37) satisfies the forward-invariance condition in Eq. (28) of the safe set $\mathcal{C}$, and is equivalent to linearizing a protective surface that was defined using an impedance variable equal to $\begin{bmatrix} I_3, & \frac{1}{\gamma} I_3 \end{bmatrix} z$ around the obstacle.*

IV. Model Predictive Variable Impedance (PVI) Controller

A linear model predictive controller was designed to vary the impedance behavior of a robot using the safety condition of Eq. (37) defined in Sec. III to allow robot obstacle avoidance for safe HRC.

A. Optimization Problem

The proposed model predictive controller solves, at every sampling step k, an optimization problem that minimizes the difference between the behavior of the robot and a reference impedance behavior defined by reference states x^r and inputs u^r throughout a prediction horizon h_p. This is equivalent to the minimization of the cost function

$$L(U_{k,p}) = \sum_{i=k+1}^{k+h_p} \Big[(x_i^r - x_i)^{\text{T}} Q (x_i^r - x_i) + (u_{i-1}^r - u_{i-1})^{\text{T}} R (u_{i-1}^r - u_{i-1}) \Big] \tag{40}$$

with $U_{k,p} = [u_k^{\text{T}}, \ldots, u_{k+h_p-1}^{\text{T}}]^{\text{T}} \in \mathbb{R}^{mh_p}$ being the sequence of computed inputs to the system throughout the control horizon (which was chosen to have the same length as the prediction horizon, $h_c = h_p$). Also, $Q \in S_{++}^{2m}$ and $R \in S_{++}^{m}$ in Eq. (40) are symmetric positive-definite matrices that penalize, respectively, the system states and inputs variation from their impedance reference at every time step.

The minimization of the cost function in Eq. (40) was subject to two types of constraints. First, the robot should exhibit impedance properties. To this purpose, the continuous-time impedance model of the robot of Eq. (8) was discretized using a zero-order-hold (ZOH) [20] sampling method

$$x_{k+j} = \Phi x_{k+j-1} + \Gamma u_{k+j-1} \tag{41}$$

$$\Phi = e^{AT_s}, \;\; \Gamma = \int_0^{T_s} e^{As} \mathrm{d}s B \tag{42}$$

with T_s being the sampling period of the system, which affects the duration of the prediction horizon.

Second, obstacle avoidance was implemented in the optimization problem as an inequality constraint to ensure that the states of the system fulfilled the linearized condition for forward-invariance of Eq. (37) of the safe set $\mathcal{C}$ at every time-step over the prediction horizon

$$A_{\text{BF}} x_{k+j} \leq {}^j b_{\text{BF}} \tag{43}$$

Remark. *Note the use of superscript ^{j} in the inequality constraint (43). This superscript highlighted that ${}^{j}b_{\mathrm{BF}}$ might take different values for each time-step $k+j$ of the prediction horizon since it would depend on the, possibly time-varying, position reference ρ_d, as seen in Eq. (39).*

As a summary, the optimization problem solved at each time-step k in the proposed Model Predictive Variable Impedance (PVI) formulation is

$$\begin{aligned} U^*_{k,p} = \min_{U_{k,p}} \; & L(U_{k,p}) \\ \text{s.t. } & x_{k+j} = \Phi x_{k+j-1} + \Gamma u_{k+j-1}, \\ & A_{\mathrm{BF}} x_{k+j} \leq {}^{j}b_{\mathrm{BF}} \; \forall \; j \in [1, \dots, h_p] \end{aligned} \tag{44}$$

B. Human-Guidance Force Estimation

In addition to the estimation of the robot motion provided by the equality constraint in Eq. (41), a prediction of human guidance can be included in the optimization problem. To this end, a linear model was chosen to describe the temporal variation of the external force throughout the prediction horizon of the MPC. In discrete time, the external force was modeled by

$$F^{\mathrm{ext}}_{k+j} = F^{\mathrm{ext}}_{k} + r_k(t_{k+j} - t_k) \tag{45}$$

where r_k is related to the estimated rate of change of this signal over the prediction horizon, which is updated at each sampling step k.

Moreover, the prediction of $F^{\mathrm{ext}}_{k+j} \; \forall \; j \in [1, \dots, h_p]$ determined the reference input sequence,

$$U^r_{k,p} = \left[(u^r_k)^{\mathrm{T}}, \dots, (u^r_{k+h_p-1})^{\mathrm{T}} \right]^{\mathrm{T}} \in \mathbb{R}^{mh_p} \tag{46}$$

used in the cost function of Eq. (40), as shown in the continuous-time input (9) of the impedance-controlled system. Additionally, the reference state sequence,

$$X^r_{k,p} = \left[(x^r_{k+1})^{\mathrm{T}}, \dots, (x^r_{k+h_p})^{\mathrm{T}} \right]^{\mathrm{T}} \in \mathbb{R}^{2mh_p} \tag{47}$$

determined by the desired impedance properties of Eq. (41) and the reference input sequence $U^r_{k,p}$.

C. Optimality

Proposition 2. *An analytic expression for the optimal solution to the optimization problem presented in Eq. (44) can be derived.*

Proof. The optimization problem of Eq. (44) could be expressed as a function of the entire sequence of states over the prediction horizon,

$$X_{k,p} = [x^{\mathrm{T}}_{k+1}, \dots, x^{\mathrm{T}}_{k+h_p}]^{\mathrm{T}} \in \mathbb{R}^{2mh_p} \tag{48}$$

Then, the equality constraint (41) is equivalent to

$$X_{k,p} = M_p U_{k,p} + N_p x_k \tag{49}$$

with $M_p \in \mathbb{R}^{2mh_p \times mh_p}$ and $N_p \in \mathbb{R}^{2mh_p \times 2m}$ being

$$M_p = \begin{bmatrix} \Gamma & 0 & \dots & 0 \\ \Phi\Gamma & \Gamma & & 0 \\ \vdots & \vdots & \ddots & \vdots \\ \Phi^{h_p-1}\Gamma & \Phi^{h_p-2}\Gamma & \dots & \Gamma \end{bmatrix}, \; N_p = \begin{bmatrix} \Phi \\ \vdots \\ \Phi^{h_p} \end{bmatrix} \tag{50}$$

Moreover, the safety condition in Eq. (43) is equivalent to

$${}^{p}A_{\mathrm{BF}} X_{k,p} \leq {}^{p}b_{\mathrm{BF}} \tag{51}$$

with ${}^{p}A_{\mathrm{BF}} \in \mathbb{R}^{h_p \times h_p}$ and ${}^{p}b_{\mathrm{BF}} \in \mathbb{R}^{h_p}$ being

$${}^{p}A_{\mathrm{BF}} = \mathrm{diag}\left([A_{\mathrm{BF}}, \dots, A_{\mathrm{BF}}]\right) \tag{52}$$

$${}^{p}b_{\mathrm{BF}} = [{}^{1}b_{\mathrm{BF}}, \dots, {}^{h_p}b_{\mathrm{BF}}]^{\mathrm{T}} \tag{53}$$

where $\mathrm{diag}(\cdot)$ forms a block diagonal matrix from a given list of matrices. Also, Eq. (51) is equivalent, in terms of the sequence $U_{k,p}$ of inputs over the prediction horizon, to

$$T U_{k,p} \leq W_1 + W_2 x_k \tag{54}$$

where

$$T = {}^{p}A_{\mathrm{BF}} M_p, \; W_1 = {}^{p}b_{\mathrm{BF}}, \; W_2 = -{}^{p}A_{\mathrm{BF}} N_p \tag{55}$$

Additionally, if these expressions are rewritten in terms of the error dynamics

$$\tilde{U}_{k,p} = U^r_{k,p} - U_{k,p}, \; \tilde{X}_{k,p} = X^r_{k,p} - X_{k,p} \tag{56}$$

the cost function of Eq. (40) is equivalent to

$$L(\tilde{U}_{k,p}) = \tilde{X}^{\mathrm{T}}_{k,p} Q_p \tilde{X}_{k,p} + \tilde{U}^{\mathrm{T}}_{k,p} R_p \tilde{U}_{k,p} \tag{57}$$

where $Q_p = \mathrm{diag}\left(\left[Q, \dots, Q\right]\right) \in \mathbb{R}^{2mh_p \times 2mh_p}$ and $R_p = \mathrm{diag}\left(\left[R, \dots, R\right]\right) \in \mathbb{R}^{mh_p \times mh_p}$ and the inequality constraint (54) could be rewritten as:

$$T_{\mathrm{e}} \tilde{U}_{k,p} \leq W_{1,\mathrm{e}} + W_{2,\mathrm{e}} \tilde{x}_k \tag{58}$$

where

$$T_{\mathrm{e}} = -T, \; W_{1,\mathrm{e}} = W_1 - U^r_{k,p} + W_2 x^r_k, \; W_{2,\mathrm{e}} = -W_2 \tag{59}$$

Finally, since the system reference ($X^r_{k,p}$ and $U^r_{k,p}$) followed the same desired impedance behavior that was imposed as an equality constraint of Eq. (41) of the optimization problem, the equality constraint in terms of the error dynamics is equivalent to

$$\tilde{X}_{k,p} = M_p \tilde{U}_{k,p} + N_p \tilde{x}_k \tag{60}$$

for M_p and N_p defined in (50).

Once the optimization problem (44) has been expressed in terms of its error dynamics sequence, it is straightforward to see that the cost function of Eq. (57), when considering the equality constraint (60), is equal to

$$L_u(\tilde{U}_{k,p}) = \tilde{U}^{\mathrm{T}}_{k,p} F \tilde{U}_{k,p} + 2\tilde{U}^{\mathrm{T}}_{k,p} G \tilde{x}_k + \tilde{x}^{\mathrm{T}}_k H \tilde{x}_k \tag{61}$$

for

$$F = M^{\mathrm{T}}_p Q_p M_p + R_p, \; G = M^{\mathrm{T}}_p Q_p N_p, \; H = N^{\mathrm{T}}_p Q_p N_p \tag{62}$$

Then, Lagrange multipliers λ_k could be used to form the Lagrangian [21]

$$\begin{aligned} L(\tilde{U}_{k,p}) = {} & \tilde{U}^{\mathrm{T}}_{k,p} F \tilde{U}_{k,p} + 2\tilde{U}^{\mathrm{T}}_{k,p} G \tilde{x}_k + \tilde{x}^{\mathrm{T}}_k H \tilde{x}_k \\ & + 2\lambda^{\mathrm{T}}_k (T_{\mathrm{e}} \tilde{U}_{k,p} - W_{1,\mathrm{e}} - W_{2,\mathrm{e}} \tilde{x}_k) \end{aligned} \tag{63}$$

By completion of squares, this expression is equal to

$$L(\tilde{U}_{k,p}) = \left(\tilde{U}_{k,p} + F^{-1}\left[G, T_{\mathrm{e}}^{\mathrm{T}}\right]\begin{bmatrix}\tilde{x}_x \\ \lambda_k\end{bmatrix}\right)^{\mathrm{T}} F \left(\tilde{U}_{k,p} + F^{-1}\left[G, T_{\mathrm{e}}^{\mathrm{T}}\right]\begin{bmatrix}\tilde{x}_x \\ \lambda_k\end{bmatrix}\right) + \tilde{x}_k^{\mathrm{T}} H \tilde{x}_k - \\ - \begin{bmatrix}\tilde{x}_k \\ \lambda_k\end{bmatrix}^{\mathrm{T}} \left(\left[G, T_{\mathrm{e}}^{\mathrm{T}}\right]^{\mathrm{T}} F^{-1}\left[G, T_{\mathrm{e}}^{\mathrm{T}}\right]\right)\begin{bmatrix}\tilde{x}_k \\ \lambda_k\end{bmatrix} - \\ -2\lambda_k^{\mathrm{T}}\left(W_{1,\mathrm{e}} + W_{2,\mathrm{e}}\tilde{x}_k\right) \tag{64}$$

Therefore, the optimal control sequence is equal to

$$\tilde{U}_{k,p}^{*} = -F^{-1}\left[G, T_{\mathrm{e},k}^{\mathrm{T}}\right]\begin{bmatrix}\tilde{x}_k \\ \lambda_k^{*}\end{bmatrix} \tag{65}$$

where only the inequality constraints that were active at time-step k were considered ($T_{\mathrm{e},k}$ and λ_k^{*}). The minimal cost function

$$\begin{aligned}\min L(\tilde{U}_{k,p}) &= L(\tilde{U}_{k,p}^{*}) \\ &= \tilde{x}_k^{\mathrm{T}}\left(H - G^{\mathrm{T}}F^{-1}G\right)\tilde{x}_k + \\ &\quad \left(\lambda_k^{*}\right)^{\mathrm{T}} T_{\mathrm{e},k} F^{-1} T_{\mathrm{e},k}^{\mathrm{T}} \lambda_k^{*}\end{aligned} \tag{66}$$

was obtained from the optimal control sequence of Eq. (65). □

D. Stability in Error Dynamics

Proposition 3. *Asymptotic stability guarantees for the error dynamics of the proposed PVI controller can be provided.*

Proof. Since the equality constraint of the optimization problem in Eq. (41) ensures that both the solution obtained from the PVI controller and the reference behavior of the system (defined by the state and input references, x^r and u^r), followed the desired robot impedance behavior, the error dynamics could be described with

$$\dot{\tilde{x}} = A(q, \dot{q})\tilde{x} + B(q)(u^r - u) \tag{67}$$

where

$$\tilde{x} = x^r - x = \left[\widetilde{\Delta\xi}^{\mathrm{T}}, \dot{\widetilde{\Delta\xi}}^{\mathrm{T}}\right]^{\mathrm{T}} \tag{68}$$

Moreover, the Lyapunov function that was used to show the global asymptotic stability for the system dynamics in Eq. (8) can also be used to show the global asymptotic stability for the system error dynamics of the proposed PVI controller by replacing x for $\tilde{x}$ in Eq. (12):

$$V(\tilde{x}, t) = \frac{1}{2}\dot{\widetilde{\Delta\xi}}^{\mathrm{T}} M_{\xi}(q)\dot{\widetilde{\Delta\xi}} + \frac{1}{2}\widetilde{\Delta\xi}^{\mathrm{T}} K \widetilde{\Delta\xi} + \alpha\Delta\xi^{\mathrm{T}} M_{\xi}(q)\dot{\widetilde{\Delta\xi}} \tag{69}$$

for analogous conditions on $\alpha > 0$ as the ones in Eq. (13). □

V. Simulations

The empirical evaluation of the PVI method was started by performing simulations with a two-dimensional double integrator system, which might be used for robot manipulators if their maximally-allowed accelerations are conservatively chosen [22], [23]. The input $u \in \mathbb{R}^2$ to this system was equal to the acceleration of the system

$$u = \ddot{\rho} \in \mathbb{R}^2 \tag{70}$$

with the position of the system being $\rho = [\rho_x, \rho_y]^{\mathrm{T}} \in \mathbb{R}^2$. Additionally, analogous to the impedance controller for the robot dynamics in Eq. (7), an impedance behavior could be achieved for the double-integrator model with

$$u = u_0 + \Delta u, \quad u_0 = K\Delta\rho - D\dot{\rho}, \quad \Delta\rho = \rho_d - \rho \tag{71}$$

such that the continuous-time impedance behavior of the system, with state vector $x = [\Delta\rho^{\mathrm{T}}, \Delta\dot{\rho}^{\mathrm{T}}]^{\mathrm{T}} \in \mathbb{R}^4$ was modeled by

$$\dot{x} = \begin{bmatrix}0_2 & I_2 \\ -K & -D\end{bmatrix} x + \begin{bmatrix}0_2 \\ -I_2\end{bmatrix}\Delta u \tag{72}$$

where $K = kI_2$ and $D = dI_2$, with $k, d > 0$.

Moreover, for the simulations performed, it was desired that a system with initial position $\rho_0 = [0, 0]^{\mathrm{T}}$ followed a trajectory determined by a constant speed of 0.4 m/s along each direction, which yielded a position reference at each discrete time-step k equal to:

$$\rho_{d,k} = \rho_{d,k-1} + 0.4\begin{bmatrix}1 \\ 1\end{bmatrix} T_s \tag{73}$$

with T_s being the discrete-sampling period of the system, which was chosen as 0.1 s for this simulation. The PVI controller of Eq. (44) was used to achieve robot obstacle avoidance, and the resulting optimization problem was solved using the convex optimization solver CVXGEN [24]. For this simulation, the obstacle was located at $\rho_{\mathrm{obs}} = \left[2, 1.5\right]^{\mathrm{T}}$ m, with a safety distance of $D_s = 0.5$ m.

Furthermore, the control-induced stiffness and damping were chosen as $k = 1$ and $d = 1/\gamma$ for $\gamma = 1.5$ and the total simulation time was 10 s. Also, regarding the parameters of the MPC optimization problem, the control and prediction horizons were chosen as $h_p = h_c = 10$, and the states and input penalization with respect to their reference in the cost function of Eq. (40) were $Q = I_4$ and $R = 0.1I_2$, respectively.

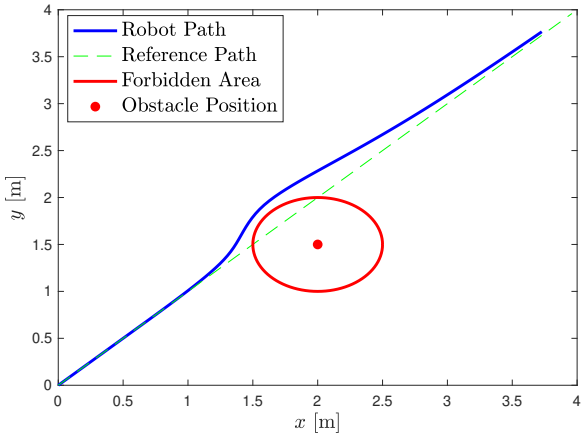

Fig. 2. Simulated path traversed by the robot compared to its reference path.

Figures 2 and 3 show the simulation results of modifying the impedance behavior of a two-dimensional double integrator for robot obstacle avoidance using PVI. Determined by the PVI controller, the system closely followed the reference until a detour was commanded to avoid the forbidden area that

surrounded the obstacle (Fig. 2). Once the commanded detour was not needed anymore for obstacle avoidance, the system was able to converge to its nominal path. Additionally, the input commanded to the system is shown in Fig. 3. The conservative acceleration values seen in this figure justified the use of a double integrator model for this simulation.

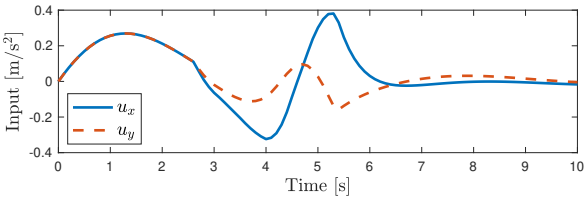

Fig. 3. Temporal evolution of the input signal throughout the simulation.

VI. Experiments

The empirical evaluation of the proposed method was extended with a series of experiments performed with a real robot in an experimental setup that allowed human–robot collaboration. The PVI solution was compared to a previous formulation [12] where prediction was not considered, to highlight the benefits of using a model-predictive scheme in these collaborative applications.

A. Experimental Setup

The experimental setup that was used to evaluate the method on a real robot consisted of a Franka Emika Panda robot [25] mounted on a table (as seen in Fig. 1). This robot has seven rotational joints, $n = 7 > 6 = m$, so, the last joint was locked at $\theta_7 = \pi/2$ rad, and only the first six joints of the robot were controlled. In addition, the controller was running at the sampling rate of the Panda robot, equal to 1 kHz, using a single PC (Intel Xeon CPU E3-1245, 3.7 GHz, 4 cores, 64-bit), and CVXGEN [24] was used to obtain the optimal control of Eq. (65).

Moreover, the nominal robot impedance that enabled HRC by allowing an operator to guide the robot was defined by a control-induced stiffness, K in Eq. (7), equal to 150 N/m for the translational degrees of freedom and equal to 10 N/rad for the rotational degrees of freedom, and a control-induced damping, D in Eq. (7), equal to $2\sqrt{K}$ for all degrees of freedom [26]. Also, the internal controller of the Franka Emika Panda robot [25] took care of the gravity compensation, and provided the remaining dynamics parameters that were needed to implement Eq. (7).

Furthermore, regarding the parameters of the MPC optimization problem for the experiments, both the control and the prediction horizons lasted 1 s, divided into ten discrete-time steps ($h_p = h_c = 10$) that were equally spaced at 0.1 s. Also, the penalization of the states and inputs with respect to their reference in the cost function of Eq. (40) was chosen as $Q = I_6$ and $R = 0.1I_3$, respectively, and all the experiments presented lasted 10 s, $t \in [0, t_{\max} = 10]$ s.

B. Robot Obstacle Avoidance in Free Motion and Influence of the Selection of γ

The behavior of the robot was evaluated for a scenario where, in the absence of external guidance force, the nominal impedance behavior of the robot would have resulted in an unmodified robot path, ρ_{un}, that collided with an obstacle, as shown in Fig. 4. Figure 4 also shows the 3D plot of the path ρ, traversed by the PVI-controlled robot. The initial position of the robot relative to its base frame was equal to $\rho_0 = [0.358, -0.2, 0.395]$ m, and the final position of the robot was equal to $\rho_{\text{F}} = \rho_0 + \Delta\rho$ for $\Delta\rho = [0.1, 0.5, 0.1]$ m. The position reference of Eq. (6) of the robot was defined to increase linearly with time

$$\rho_d(t) = \rho_0 + \frac{\Delta\rho}{t_{\max}} t \tag{74}$$

Also, the obstacle was placed at $\rho_{\text{obs}} = [0.4, 0.0, 0.45]$ m and the safety distance was equal to $D_s = 0.05$ m.

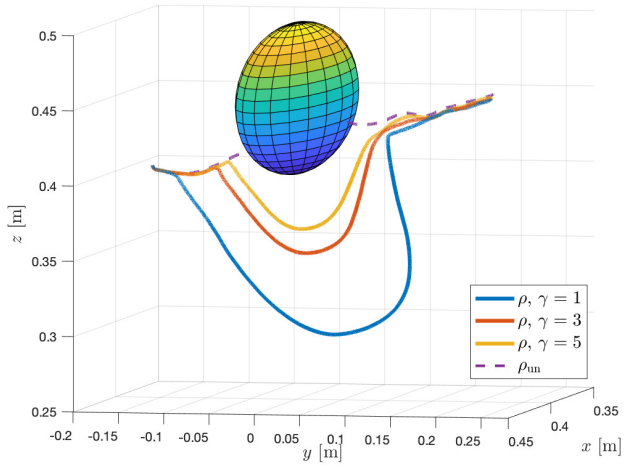

Fig. 4. 3D rendering of the path ρ traversed by the end-effector of the MPC-controlled robot for different values of γ (28). The unmodified path, ρ_{un}, showed the path that the robot would follow with its nominal impedance behavior. The plotted sphere was centered at the obstacle position ρ_{obs} and its radius was equal to the safety distance D_s.

As seen in Fig. 4, the PVI-based strategy was able to avoid any collision between the robot and the obstacle. Additionally, this controller allowed that the path followed by the robot converged toward the unmodified path, ρ_{un}, once the robot passed the obstacle. Moreover, it is also observed in Fig. 4 that the selection of γ in the forward-invariance condition in Eq. (28) of the safe set $\mathcal{C}$ had a significant influence on the behavior of the PVI-controlled robot, *i.e.*, a higher value of γ yielded a less conservative solution, where the robot got closer to the obstacle during the trajectory execution. Indeed, this observation was supported when the temporal evolution of the barrier function h of Eq. (26) was analyzed, as depicted in Fig. 5. Even though the PVI-solution avoided the obstacle for all the analyzed values of γ, it can be seen in Fig. 5 that the robot motion was less conservative for higher values of γ. This was also observed when analyzing the minimum distance between the robot and the obstacle ($D_{\min}$), and the duration

of the deviation from the nominal impedance behavior (t_{dur}), as seen in Table I.

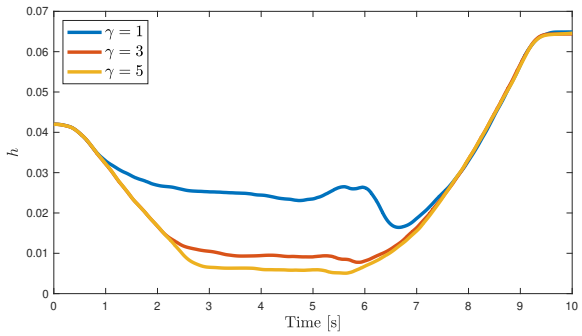

Fig. 5. Temporal evolution of the barrier function h in Eq. (26) throughout the experiment for different values of γ in Eq. (28).

TABLE I
PERFORMANCE METRICS AS A FUNCTION OF γ

	$\gamma = 1$	$\gamma = 3$	$\gamma = 5$
D_{min}	13.7 cm	10.1 cm	8.7 cm
t_{dur}	6.2 s	4.5 s	3.6 s

Furthermore, Fig. 6 shows the difference in the commanded forces to the robot, F in Eq. (2), along each Cartesian direction depending on the choice of γ compared to the unperturbed impedance solution with no robot obstacle avoidance. Selecting a higher value of γ allowed the robot to achieve a less conservative solution where a smaller deviation with respect to the nominal impedance behavior, both in terms of the amount of time deviating from the nominal impedance behavior, and in terms of the magnitude of the deviation, was observed.

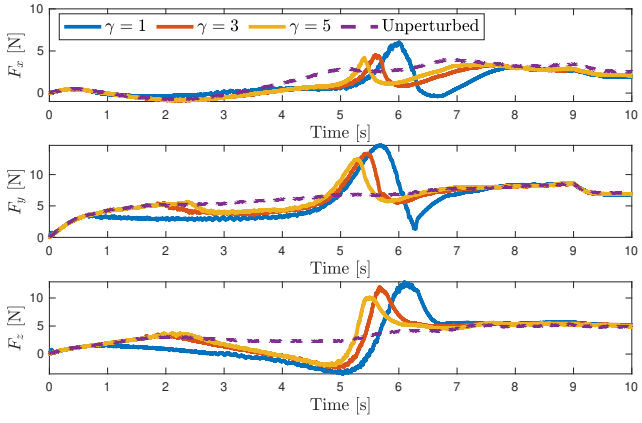

Fig. 6. Commanded force F in Eq. (2) to the robot along each Cartesian direction x, y, z throughout the experiment for different values of γ in Eq. (28).

C. Comparison with a 1-step Solution in Free Motion

The collision-avoidance situation in free motion described in Sec. VI-B was used for comparing the PVI solution with respect to a 1-step formulation [12], which was also executed at the sampling frequency of the robot, *i.e.*, 1 kHz. The same value of $\gamma = 5$ in Eq. (28) was used for both formulations. The advantages of considering a prediction of the robot motion for robot obstacle avoidance were apparent in this situation.

First, the PVI-controlled robot was able to stay less time at risk by acting earlier to modify the nominal impedance behavior, as shown in Fig. 7, where the temporal evolution of the velocity of the robot end-effector is depicted. It can be seen in Fig. 7 that before $t = 4$ s, the PVI-controlled robot had started to move away from the obstacle, while the 1-step controller commanded the robot to keep a velocity close to zero in all its components until after $t = 6$ s.

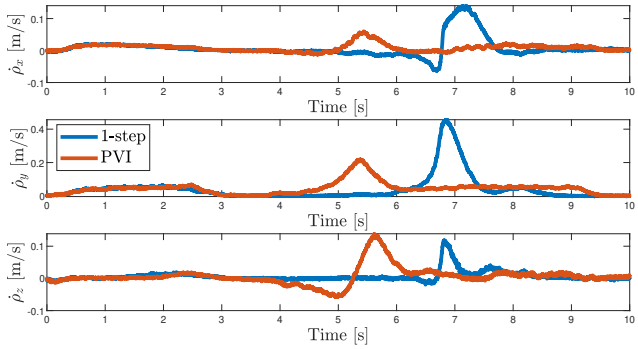

Fig. 7. Temporal evolution of the velocity of the robot end-effector along each Cartesian direction x, y, z for the PVI-controlled robot compared to a 1-step controller formulation [12].

Moreover, the robot-motion prediction, combined with the utilization of the temporal evolution of the desired impedance behavior of the robot throughout the prediction horizon, allowed the PVI controller to reduce the trajectory error. This is seen in Fig. 8, which showed a comparison of the trajectory of the PVI formulation and the 1-step formulation with respect to the unperturbed impedance behavior of the robot, *i.e.*, without collision avoidance. The PVI controller was able to provide a closer tracking of the reference impedance trajectory, which was quantified using the Mean Absolute Error (MAE) between the nominal (unperturbed) and the actual position of the robot end-effector

$$\text{MAE}(\rho) = \frac{\sum_{k=0}^{N} |\rho_{\text{un},k} - \rho_k|}{N} \tag{75}$$

where $N = f \cdot t_{\text{max}}$ and $f = 1000$ Hz since experimental data were recorded in these experiments at the sampling rate of the Panda robot (1 kHz). For the trajectory described in Fig. 8, the position MAE of the 1-step controller was 0.0553 m, whereas the position MAE of the PVI controller was 0.0185 m, which implied a reduction of 66.5% of the position MAE. Also, for the PVI controller, the deviation from the nominal trajectory lasted 3.8 s, compared to the 5.8 s that it lasted for the 1-step controller.

Additionally, it should be highlighted that not only did the PVI controller execute a collision-avoidance strategy earlier than the 1-step alternative, but also, since it was able to consider a prediction of the robot motion and the desired robot behavior throughout its prediction horizon, the PVI controller

could pursue a different, and better, path for obstacle avoidance than its 1-step counterpart.

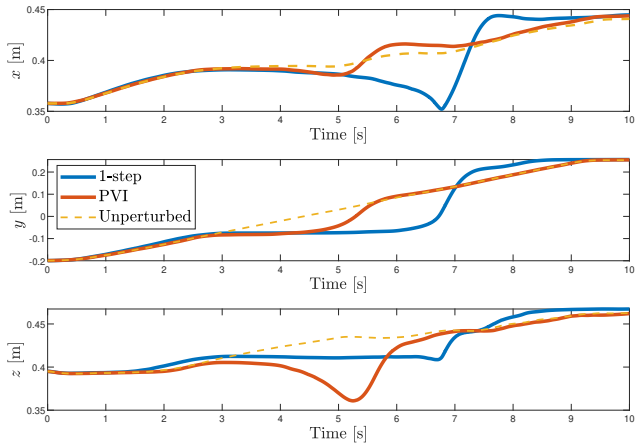

Fig. 8. Trajectory followed by the robot end-effector along Cartesian direction x, y, z for both the predictive controller (PVI) and a 1-step controller [12], with respect to the unperturbed, nominal, impedance behavior.

D. External Force Prediction

An additional advantage of the PVI strategy is that it could include a prediction model of the external force applied to the robot by a human operator guiding it throughout its prediction horizon, which could be used to improve the performance of the system. The low-complexity linear model for external force prediction introduced in Sec. IV-B was evaluated and compared to a model that considered a constant external force throughout the entire prediction horizon. For this constant-force model, both the value of the external force at the current time and a zero value of the external force were considered as its constant value.

Additionally, the linear model could be estimated based on sensor data available at the estimation time

$$\hat{F}^{\text{ext}}_{t|t_k} = F^{\text{ext}}_{t_k} + r_k(t - t_k) \tag{76}$$

where $\hat{F}^{\text{ext}}_{t|t_k}$ is the prediction made at time t_k of the value of the external force at time t. The slope r_k of the linear model was chosen proportional to the Cartesian acceleration of the robot at time t_k, which was recalculated at the sampling rate of the robot using a least-squares method that considered the previous $N_r = 10$ values of the Cartesian acceleration as a moving average to avoid the detrimental effects of measurement noise,

$$r_k \propto \frac{\sum_{i=1}^{N_r}(t_{k-i} - \bar{t}_{N_r})(\ddot{\rho}_{k-i} - \bar{\ddot{\rho}}_{N_r})}{\sum_{i=1}^{N_r}(t_{k-i} - \bar{t}_{N_r})^2} \tag{77}$$

where $\bar{t}_{N_r}$ and $\bar{\ddot{\rho}}_{N_r}$ are, respectively, the averages of t_{k-i} and $\ddot{\rho}_{k-i}$ for $i \in [1, \ldots, N_r]$.

Moreover, the accuracy of the different models proposed to estimate the guidance force was studied for a situation where an operator was trying to move the robot away from its nominal trajectory. Because of the impedance behavior of the robot with respect to its reference, the operator would be required to apply a greater force to move the robot away from its nominal trajectory, the further away the robot was positioned with respect to this trajectory. Therefore, the external force would be expected to increase linearly in this scenario. To evaluate the accuracy of these models used to predict the external force, the MAE between the predicted and the actual external force was computed for each time step j of the prediction horizon h_p as

$$\text{MAE}(\hat{F}^{\text{ext}}_j) = \frac{\sum_{k=0}^{N} \left| \hat{F}^{\text{ext}}_{k+0.1f\cdot j|k} - F^{\text{ext}}_{k+0.1f\cdot j} \right|}{N} \tag{78}$$

where $j = [1, \ldots, h_p]$, $N = f \cdot t_{\max}$, and $f = 1000$ Hz because of the sampling rate of the robot, as in Eq. (75). The external-force MAE for the different estimation models is shown in Fig. 9 for an experiment where the guidance force was exerted along the negative z-direction.

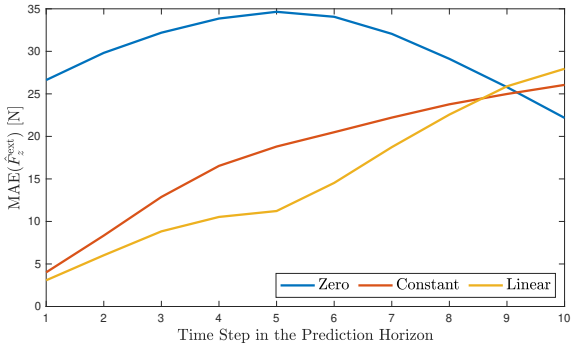

Fig. 9. Mean Absolute Error (MAE) of the predicted external force along the negative z-direction throughout the PVI prediction horizon for different models.

As seen in Fig. 9, the linear model significantly outperformed the constant model that used the initial external force measurement as its constant value. Also, both of these models clearly outperformed the constant zero model, except for the last time-steps of the prediction horizon, where the current state of the robot was not useful for predicting the external force. Moreover, the advantage of using the linear model with respect to the constant model became more evident when analyzing the temporal evolution of the predicted external force in each of these two models compared to the measured force. This is seen in Fig. 10, where the results of the prediction of the human guidance situation for a prediction time of 0.5 s ($j = 5$) are shown.

As expected, the constant model appeared as a delayed version of the measured external force signal, with a delay equal to the prediction time, which was equal to 0.5 s in Fig. 10. On the other hand, the linear model was able to achieve a faster response to the changes in the measured external force, which might be useful for safety-critical scenarios.

E. Comparison with a 1-step Solution during Human Guidance

To obtain a fair comparison between the proposed PVI controller and a 1-step controller in a human-guidance situation, the same external force should be applied to the robot for each

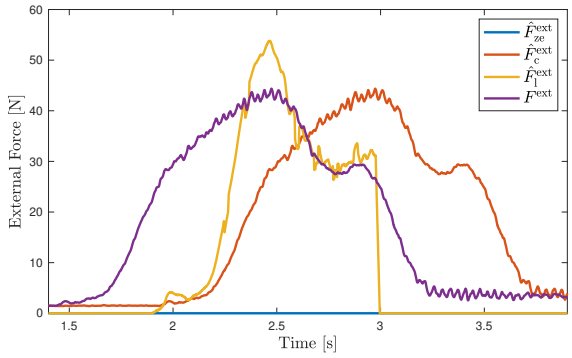

Fig. 10. Predicted external force for a human-guidance situation along the negative z-direction. F^{ext} denotes the measured external force and $\hat{F}_{\text{ze}}^{\text{ext}}$, $\hat{F}_{\text{c}}^{\text{ext}}$, and $\hat{F}_{\text{l}}^{\text{ext}}$ denote the zero, constant, and linear predictions of the external force, respectively, for a prediction time of 0.5 s.

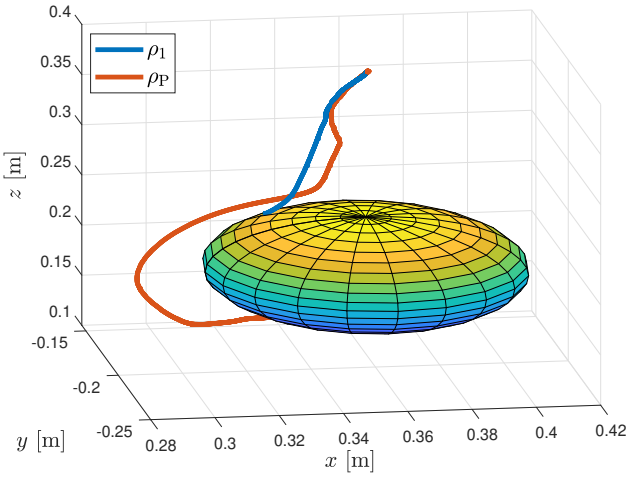

Fig. 11. 3D rendering of the path traversed by the robot end-effector controlled using PVI, ρ_{P}, compared to the path traversed by the robot end-effector controlled using a 1-step controller, ρ_1, when a simulated guidance force f_s in (79) was applied to the robot along the negative z-direction. The plotted sphere was centered at the obstacle position ρ_{obs} and its radius was equal to the safety distance D_s.

of these two controllers. To this end, a simulated guidance force $f_s(t)$ was used. The simulated force $f_s(t)$ consisted of a sinusoidal signal with an amplitude of 30 N and a period of 3 s (to resemble the external force originated from human guidance seen in Fig. 10), and was applied to the robot along the negative z-direction

$$f_s(t) = -30\sin(\frac{2\pi}{3}(t-2)),\ t \in [2, 3.5]s \tag{79}$$

Moreover, the trajectory used to compare the PVI solution to a 1-step controller in this human-guidance situation considered that the initial position of the robot was $\rho_0 = [0.357, -0.2, 0.395]$ m, and that the desired position of the robot varied linearly (Eq. (74)) during 10 s until reaching the final reference position $\rho_{\text{F}} = [0.357, -0.2, 0.1]$ m. Additionally, the obstacle was positioned to intersect with the nominal trajectory: $\rho_{\text{obs}} = [0.357, -0.2, 0.2]$ m with radius equal to $D_s = 0.05$ m.

Figure 11 shows the 3D plot of the path ρ_{P} traversed by the robot controlled using the PVI formulation, compared with the path obtained when using a 1-step controller alternative without predictive capabilities, ρ_1. It can be seen that, for the human-guidance scenario illustrated in Fig. 11, even though the 1-step controller started deviating from the nominal trajectory earlier than the PVI controller ($t = 1.4$ s for the 1-step controller versus $t = 2.35$ s for the PVI controller), the longer-time prediction of the robot motion and the guidance force allowed the PVI-controlled robot to circuit the obstacle. On the contrary, whereas when the robot was controlled using a 1-step formulation it got stuck in the surroundings of the obstacle.

F. Human Guidance for an Assembly Task in the Presence of an Obstacle

The proposed PVI controller was evaluated in a collaborative scenario that involved human guidance with an obstacle present in the shared workspace. Manual guidance of a robot could be used to correct the Cartesian reference, ξ_d in Eq. (6), for a robot assembly task after the requirements of this task had changed, *e.g.*, a peg-in-hole task where the position of the hole had changed. Additionally, a camera mounted on the same table as the robot was present in the shared workspace to be used for visual quality inspection of the workpieces involved in the assembly [27]. From the human-guidance perspective, an accidental collision between the camera and the guided robot should be avoided to refrain from any damage to the camera or the other workpieces and to obtain a valid manual correction for the robot trajectory. An overview of the experimental scenario is shown in Fig. 12.

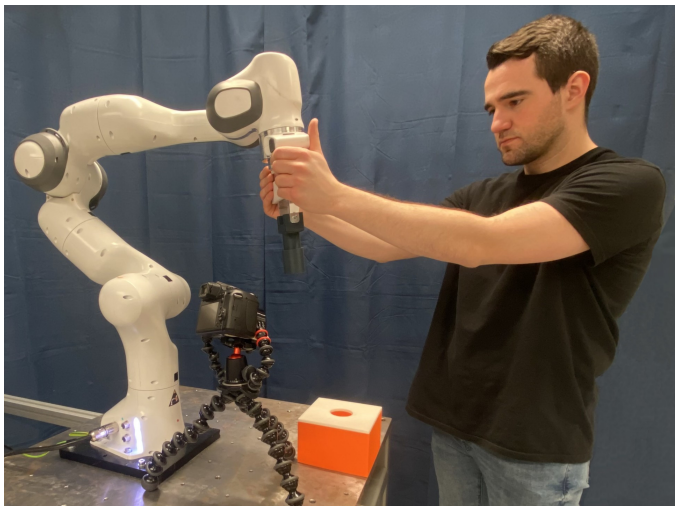

Fig. 12. A human–robot collaborative scenario where the operator was guiding the robot to teach a peg-in-hole task in the presence of an obstacle (a camera).

In this experimental scenario, the human operator was instructed to manually guide the robot to achieve its task completion, *i.e.*, the insertion of the peg in the hole, in the shortest time and path possible. However, the presence of the camera in the shared workspace would condition the manual

trajectory correction. The initial position of the robot relative to its base frame was equal to $\rho_0 = [0.3, -0.19, 0.683]$ m, and the position reference of the robot varied linearly (Eq. (74)) during 10 s until reaching the final reference position $\rho_{\text{F}} = [0.087, 0.34, -0.55]$ m. Also, the camera was placed at $\rho_{\text{obs}} = [0.38, 0.0, 0.33]$ m and the safety distance was equal to $D_s = 0.05$ m.

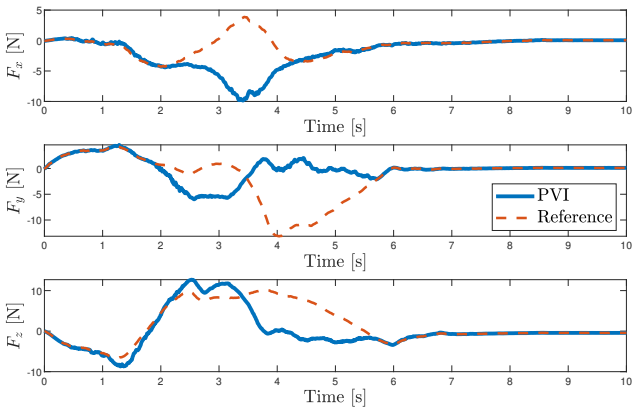

Fig. 13. Input force, F in Eq. (2), commanded to the robot by the PVI controller of Eq. (44) compared to the reference robot impedance behavior in Eq. (7) for an assembly task in the presence of an obstacle.

A comparison between the input force, F in Eq. (2), commanded to the robot when using the proposed PVI controller, and the reference robot impedance behavior for this collaborative scenario was shown in Fig. 13. It can be seen in Fig. 13 that the PVI controller allowed the robot to behave in an equal manner to the reference robot impedance behavior, until a force input variation was necessary to avoid that the peg would invade the safety distance with respect to the camera. Then, it is also shown in Fig. 13 that after the manually-guided robot stopped being at a risk-of-collision situation, the PVI controller allowed the robot to resume the reference robot impedance behavior.

Moreover, the external force recorded from human manual guidance for this collaborative scenario is shown in Fig. 14. The response of the human operator to the robot impedance variation commanded by the PVI controller can be seen in Fig. 14. Additionally, the prediction of the external force obtained using the linear model in Eqs. (76) and (77) is shown in Fig. 14 for a time ($t = 1.5$ s) when the PVI controller started to command a robot impedance that differed from its reference to achieve obstacle avoidance. It can be observed in Fig. 14 that the linear model accurately predicted (with a MAE at $t = 1.5$ s equal to 1.4 N for the entire prediction horizon) the guidance force applied by the human operator at this time.

Furthermore, the optimization problem formulated in Eq. (44) for the proposed PVI controller took on average 95.8 μs to solve for this experiment, with a standard deviation of 20.6 μs, using a single PC with the hardware specifications described in Sec. VI-A.

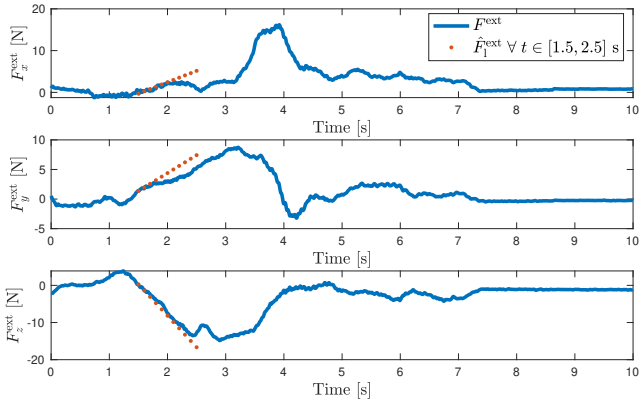

Fig. 14. External force recorded from the manual correction for an assembly task in the presence of an obstacle, and prediction at time $t = 1.5$ for the external force between $t = 1.5$ s and $t = 2.5$ s using the linear model in Eqs. (76) and (77).

VII. Discussion

In this paper, we have proposed an approach to include SCBFs in a linear MPC strategy so that a longer-time horizon prediction could be considered for safety in HRC. A comparison of the proposed method with alternative methods found in literature is discussed in this section. Also, possible limitations and extensions of the proposal are commented.

A. Comparison of the Proposal with Alternative Methods

The advantages in terms of safety obtained by considering a prediction of both the motion of the controlled robot manipulator and the human collaborator, compared to 1-step formulations [12], were shown in the experimental evaluation presented in Sec. VI. First, this prediction allowed a reduction of the trajectory error and decreased the time where a risk of obstacle collision was present. Additionally, the prediction capabilities of the proposed method prevented that the controlled robot would get stuck near an obstacle and allowed the robot to converge to its nominal trajectory after the obstacle.

Moreover, the linear MPC considered in our method satisfied the forward-invariance condition of Eq. (28) for the set of robot states that guaranteed safety during HRC, and resulted in a convex quadratic optimization problem that was solved within the control frequency of a real robot, *i.e.*, in less than 1 ms, which is significantly faster than the computational time of previously proposed nonlinear, nonconvex, MPC formulations, *i.e.*, around 40 Hz [13] and 35 Hz [14]. Also, multi-layer strategies where a slow nonlinear MPC solution was combined with a faster 1-step quadratic optimization problem solved at the control frequency of a robot (400 Hz in [13]), would not allow the use of a longer-time prediction at a fast rate to rapidly adapt to changes in the robot environment.

Additionally, the control signal obtained from nonlinear MPC would depend on the characteristics of the problem, whereas, as shown in Sec. IV-C, optimality was guaranteed in our proposal under linearity assumptions on human guidance and linearized robot dynamics, to achieve convexity in the

optimization problem formulated in Eq. (44). It becomes apparent that inaccuracies occurring when modeling the dynamic behavior of the robot and the manual robot guidance might compromise the performance of the proposal. However, in Sec. VI, the proposed formulation that includes such linearity assumptions was experimentally evaluated in robot obstacle avoidance scenarios, and suitable results were obtained both in the presence of manual robot guidance and in its absence.

Furthermore, previous contributions also considered varying the impedance behavior of a robot using MPC, although they did not integrate SCBFs to enforce safety constraints [28], [29]. Additionally, contrary to the proposed method, the dynamics of the robot was not considered in the problem constraints of these MPC formulations, and only the robot kinematics were considered. Disregarding the robot dynamics in this context was shown to cause potential safety violations [11], critical in human–robot collaborative scenarios. Also, the computational time achieved in [28], [29] caused their implementation executing at slow frequencies and/or considering only a small number of discrete time-steps in their prediction horizons.

B. Possible Limitations and Extensions of the Proposal

The guidance force that would be exerted by a human operator cannot always be predicted. The experimental validation provided in Sec. VI showed how a basic linear model could be used to predict the temporal variation of the external force signal based on sensor data available at computation time. The mass-spring-damper behavior imposed by the nominal impedance controller in Eq. (6) defined the relationship between the human guidance force and the robot deviation from its reference trajectory which motivated the selection of this linear model. However, the sensor data available might not always provide an accurate prediction, *e.g.*, it can be seen in Fig. 10, how the external-force data recorded before human interaction had started could not be used to predict the increase in external force shown in this figure. Additionally, an accurate prediction of early instances of human guidance force was achieved using this linear model for a collaborative scenario in the presence of an obstacle, as shown in Fig. 14. Accurately predicting such increases in guidance force would allow anticipatory action for safety-critical scenarios.

However, the prediction for other instances of human guidance might not be as accurate, as shown in Fig. 9, which provided the external force MAE for an entire human guidance event. In addition, the complexity of pHRI in industrial environments might exceed the guidance force scenarios considered when evaluating the proposed method. For example, they could involve unexpected or accidental human–robot interactions. The reduced computational times achieved by the proposed method would be advantageous in these, possibly rapidly-changing, scenarios. Nevertheless, more complex strategies that incorporate further information regarding the intention of the human operator [4], [30], and/or consideration of biomechanical models of the human operator and measure the corresponding muscle activity [31], could be integrated with our method to improve the prediction of physical human–robot interaction.

Moreover, even though the reference trajectory in the experiments was chosen as a straight line with constant speed, the nominal impedance dynamics, shown in Eq. (8), resulted in a PVI reference velocity of variable speed. This can be seen in the trajectory plot of Fig. 8 (yellow dashed line). Additionally, the proposed method provided valid empirical results under curved trajectories with non-constant speed. These variations in speed were induced by the application of the proposed method for obstacle avoidance in earlier time-steps of the experiments, as seen in the 3D path rendering of Fig. 4 and in the velocity plot of Fig. 7. For these reasons, the proposed method should remain valid for more complex reference trajectories, especially since such trajectories would be considered in the optimization problem of the PVI method, as seen in Eq. (41).

Furthermore, the empirical evaluation of the proposed PVI method in Secs. V and VI considered a fixed obstacle, *i.e.*, ρ_{obs} in Eqs. (38) and (39) would be constant. However, the proposed method would be able to encode a position-varying obstacle in its optimization problem, as seen in Eq. (43). An overview of methods to detect the obstacle motion and suggested additional sensors needed for this was provided in [32]. Additionally, the aforementioned fast implementation of the proposed PVI method would be beneficial to handle possible inaccuracies in the modeling of obstacle motion.

VIII. Conclusion

Safety in HRC can be improved by considering a longer prediction time horizon of the motion of the controlled robot and the human-collaborator guidance. To this purpose, stable impedance behavior of a robot manipulator was varied by including linearized SCBFs for robot obstacle avoidance in a linear MPC strategy that ensured optimality. Our MPC-based proposal was evaluated in experiments using a real robot manipulator that was controlled at a fast rate (1 kHz) to allow fast reaction to changes occurring in the robot environment. These experiments showed that adding prediction capabilities to a robot controller led to a reduced time at risk of collision, improved obstacle bypassing, and decreased the trajectory error caused by obstacle avoidance.

References

[1] C. Schou, J. Damgaard, S. Bøgh, and O. Madsen, "Human-robot interface for instructing industrial tasks using kinesthetic teaching," in *IEEE Int. Symp. Robotics (ISR)*, Seoul, Korea, Oct. 19–27, 2013, pp. 1–6.

[2] A. Cencen, J. C. Verlinden, and J. Geraedts, "Design methodology to improve human-robot coproduction in small-and-medium-sized enterprises," *IEEE/ASME Trans. Mechatronics*, vol. 23, no. 3, pp. 1092–1102, 2018.

[3] S. Wrede, C. Emmerich, R. Grünberg, A. Nordmann, A. Swadzba, and J. Steil, "A user study on kinesthetic teaching of redundant robots in task and configuration space," *J. Human-Robot Interaction*, vol. 2, no. 1, pp. 56–81, 2013.

[4] T. Liu, E. Lyu, J. Wang, and M. Q.-H. Meng, "Unified intention inference and learning for human–robot cooperative assembly," *IEEE Trans. Automation Science and Engineering*, vol. 19, no. 3, pp. 2256–2266, 2021.

[5] N. Hogan, "Impedance control: An approach to manipulation: Parts I–III," *J. Dynamic Syst., Measurement, and Control*, vol. 107, no. 1, pp. 1–24, 1985.

[6] R. Johansson and M. W. Spong, "Quadratic optimization of impedance control," in *IEEE Int. Conf. Robotics and Automation (ICRA)*, San Diego, USA, Mar. 8–13, 1994, pp. 616–621.
[7] A. D. Ames, S. Coogan, M. Egerstedt, G. Notomista, K. Sreenath, and P. Tabuada, "Control barrier functions: Theory and applications," in *European Control Conference (ECC)*. Naples, Italy: IEEE, Jun. 25–28, 2019, pp. 3420–3431.
[8] C. T. Landi, F. Ferraguti, S. Costi, M. Bonfè, and C. Secchi, "Safety barrier functions for human-robot interaction with industrial manipulators," in *European Control Conference (ECC)*. Naples, Italy: IEEE, Jun. 25–28, 2019, pp. 2565–2570.
[9] A. Singletary, S. Kolathaya, and A. D. Ames, "Safety-critical kinematic control of robotic systems," *IEEE Control Systems Letters*, vol. 6, pp. 139–144, 2021.
[10] F. Ferraguti, M. Bertuletti, C. T. Landi, M. Bonfè, C. Fantuzzi, and C. Secchi, "A control barrier function approach for maximizing performance while fulfilling to ISO/TS 15066 regulations," *IEEE Robotics and Automation Letters*, vol. 5, no. 4, pp. 5921–5928, 2020.
[11] M. Rauscher, M. Kimmel, and S. Hirche, "Constrained robot control using control barrier functions," in *IEEE/RSJ Int. Conf. Intelligent Robots and Systems (IROS)*. Daejeon, Korea: IEEE, Oct. 9–14, 2016, pp. 279–285.
[12] J. M. Salt-Ducaju, B. Olofsson, A. Robertsson, and R. Johansson, "Robot Cartesian compliance variation for safe kinesthetic teaching using Safety Control Barrier Functions," in *IEEE Int. Conf. Automation Science and Engineering (CASE)*. Mexico City, Mexico: IEEE, Aug. 20–24, 2022, pp. 2259–2266.
[13] R. Grandia, A. J. Taylor, A. D. Ames, and M. Hutter, "Multi-layered safety for legged robots via control barrier functions and model predictive control," in *IEEE Int. Conf. Robotics and Automation (ICRA)*, Xi'an, China, 31 May–4 Jun. 2021, pp. 8352–8358.
[14] J. Zeng, B. Zhang, and K. Sreenath, "Safety-critical model predictive control with discrete-time control barrier function," in *American Control Conference (ACC)*. New Orleans, LA, USA: IEEE, May 25–28, 2021, pp. 3882–3889.
[15] B. Siciliano and O. Khatib, *Springer Handbook of Robotics*. Springer, Berlin, 2016.
[16] O. Khatib, "A unified approach for motion and force control of robot manipulators: The operational space formulation," *IEEE J. Robotics and Automation*, vol. 3, no. 1, pp. 43–53, 1987.
[17] S. Chiaverini, B. Siciliano, and O. Egeland, "Review of the damped least-squares inverse kinematics with experiments on an industrial robot manipulator," *IEEE Trans. Control Systems Technology*, vol. 2, no. 2, pp. 123–134, 1994.
[18] C. Ott, *Cartesian impedance control of redundant and flexible-joint robots*. Springer, Berlin, 2008.
[19] V. Santibáñez and R. Kelly, "Strict Lyapunov functions for control of robot manipulators," *Automatica*, vol. 33, no. 4, pp. 675–682, 1997.
[20] K. J. Åström and B. Wittenmark, *Computer-Controlled Systems: Theory and Design*. Courier Corporation, North Chelmsford, MA, USA, 2013.
[21] R. Johansson, *Model-Based Predictive and Adaptive Control*. Lund, Sweden: KFS Studentbokhandel, January 2020.
[22] B. Bäuml, T. Wimböck, and G. Hirzinger, "Kinematically optimal catching a flying ball with a hand-arm-system," in *IEEE/RSJ Int. Conf. Intelligent Robots and Systems (IROS)*, Taipei, Taiwan, Oct. 18–22, 2010, pp. 2592–2599.
[23] M. Ghazaei Ardakani, B. Olofsson, A. Robertsson, and R. Johansson, "Model predictive control for real-time point-to-point trajectory generation," *IEEE Trans. Automation Science and Engineering*, vol. 16, no. 2, pp. 972–983, Apr. 2019.
[24] J. Mattingley and S. Boyd, "CVXGEN: A code generator for embedded convex optimization," *Optimization and Engineering*, vol. 12, no. 1, pp. 1–27, 2012.
[25] *Panda – Data Sheet*, Franka Emika, 2019.
[26] M. Karlsson, A. Robertsson, and R. Johansson, "Convergence of dynamical movement primitives with temporal coupling," in *European Control Conference (ECC)*, Limassol, Cyprus, Jun. 12–15, 2018, pp. 32–39.
[27] L. Zhou, L. Zhang, and N. Konz, "Computer vision techniques in manufacturing," *IEEE Trans. Systems, Man, and Cybernetics: Systems*, vol. 53, no. 1, pp. 105–117, 2022.
[28] Z. Jin, D. Qin, A. Liu, W.-a. Zhang, and L. Yu, "Model predictive variable impedance control of manipulators for adaptive precision-compliance tradeoff," *IEEE/ASME Trans. Mechatronics*, vol. 28, no. 2, pp. 1174–1186, 2022.
[29] M. Bednarczyk, H. Omran, and B. Bayle, "Model predictive impedance control," in *IEEE Int. Conf. Robotics and Automation (ICRA)*, Paris, France, 31 May–31 Aug. 2020, pp. 4702–4708.
[30] C. Y. Wong, L. Vergez, and W. Suleiman, "Vision-and tactile-based continuous multimodal intention and attention recognition for safer physical human–robot interaction," *IEEE Trans. Automation Science and Engineering*, 2023.
[31] L. Peternel and A. Ajoudani, "After a decade of teleimpedance: A survey," *IEEE Trans. Human-Machine Systems*, vol. 53, no. 2, pp. 401–416, 2023.
[32] Z. Saleem, F. Gustafsson, E. Furey, M. McAfee, and S. Huq, "A review of external sensors for human detection in a human robot collaborative environment," *J. Intelligent Manufacturing*, pp. 1–25, 2024.

Julian M. Salt Ducaju received the B.Sc. and M.Sc. degree in aeronautical engineering from the Polytechnic University of Valencia (UPV), Valencia, Spain, in 2016 and 2018, respectively. In 2024, he received his Ph.D. degree in Robotics and Automatic Control from the Department of Automatic Control, LTH, Lund University, Sweden. His research interests include physical Human-Robot Interaction (pHRI) and force control for robots.

Björn Olofsson received the M.Sc. degree in Engineering Physics in 2010 and the Ph.D. degree in Automatic Control in 2015, both from Lund University, Sweden. He is currently an Associate Professor at the Department of Automatic Control, Lund University, Sweden, and also affiliated with the Department of Electrical Engineering, Linköping University, Sweden. His research includes motion control for robots and vehicles, optimal control, system identification, and statistical sensor fusion.

Rolf Johansson received the Master-of-Science degree in Technical Physics in 1977, the Bachelor-of-Medicine degree in 1980, the doctorate in control theory 1983, and received the Doctor-of-Medicine degree (M.D.) in 1986, all from Lund University. He was appointed Professor in 1999. From 1993, he was Director of Robotics Laboratory at Lund University. He is IEEE Fellow; Member of Bárány Society, and Fellow of the Royal Physiographic Society, Section of Medicine.

Rolf Johansson was awarded the 1995 biomedical engineering prize (the Ebeling Prize) of the Swedish Society of Medicine for distinguished contribution to the study of human balance through application and development of system analysis and robotics. He was co-recipient of *EURON Technology Transfer Award 2004, 2007*, and *ICRA2012 Best Automation Paper Award*. He is Assoc. Editor of *Intelligent Service Robotics* and *Int. J. Adaptive Control & Signal Processing* as well as Editor of *Mathematical Biosciences*. In 1993 he published the book *System Modeling and Identification*, Prentice Hall, Englewood Cliffs, NJ.